Observation of Beat Oscillation Generation by Coupled Waves Associated with Parametric Decay during Radio Frequency Wave Heating of a Spherical Tokamak Plasma

Yoshihiko Nagashima,[1,*] Takuya Oosako,[1] Yuichi Takase,[1] Akira Ejiri,[1] Osamu Watanabe,[1] Hiroaki Kobayashi,[1] Yuuki Adachi,[1] Hiroshi Tojo,[2] Takashi Yamaguchi,[1] Hiroki Kurashina,[1] Kotaro Yamada,[1] Byung Il An,[3] Hiroshi Kasahara,[4] Fujio Shimpo,[4] Ryuhei Kumazawa,[4] Hiroyuki Hayashi,[1] Haduki Matsuzawa,[1] Junichi Hiratsuka,[3] Kentaro Hanashima,[1] Hidetoshi Kakuda,[3] Takuya Sakamoto,[1] and Takuma Wakatsuki[3]

[1]*Graduate School of Frontier Sciences, The University of Tokyo, Kashiwa-shi, Chiba 277-8561, Japan*
[2]*Naka Fusion Institute, Japan Atomic Energy Agency, Naka-shi, Ibaraki 311-0193, Japan*
[3]*Graduate School of Science, The University of Tokyo, Kashiwa-shi, Chiba 277-8561, Japan*
[4]*National Institute for Fusion Science, Toki-shi, Gifu 509-5292, Japan*

(Received 11 September 2009; published 16 June 2010)

We present an observation of beat oscillation generation by coupled modes associated with parametric decay instability (PDI) during radio frequency (rf) wave heating experiments on the Tokyo Spherical Tokamak-2. Nearly identical PDI spectra, which are characterized by the coexistence of the rf pump wave, the lower-sideband wave, and the low-frequency oscillation in the ion-cyclotron range of frequency, are observed at various locations in the edge plasma. A bispectral power analysis was used to experimentally discriminate beat oscillation from the resonant mode for the first time. The pump and lower-sideband waves have resonant mode components, while the low-frequency oscillation is exclusively excited by nonlinear coupling of the pump and lower-sideband waves. Newly discovered nonlocal transport channels in spectral space and in real space via PDI are described.

DOI: 10.1103/PhysRevLett.104.245002 PACS numbers: 52.35.Mw, 52.50.Qt, 52.55.Fa

Investigation of linear or nonlinear transport channels is important for understanding structural formation in nonlinear and nonequilibrium systems in nature and the laboratory. For instance, recent studies of transport by plasma turbulence have highlighted couplings among multiscale turbulence including mesoscale secondary instabilities excited by microscale turbulence in plasmas [1,2]. The coupling is connected with the elementary parametric process [3], which is a representative nonlinear phenomenon widely observed in various fields and is linked to structural formation such as harmonic generation in nonlinear optics [4], solar wind acceleration in astrophysical or solar plasmas [5], and anomalous heating via parametric decay instability in laboratory or fusion plasmas [6].

Parametric decay instability (PDI) [7], in which a large amplitude pump wave electric field excites the lower-sideband (LSB) wave and the low-frequency quasimode via electrostatic ponderomotive force and Lorentz force, has been studied extensively both theoretically and experimentally, and is reviewed in Ref. [6]. In addition, the requirement for high wave heating efficiency has accelerated recent PDI studies in spherical tokamaks [8,9]. PDI is a local nonlinear process with the scale length of the pump wave power profile. However, nonlocal effects can occur over a distance larger than this scale length. For instance, when the LSB wave is a resonant mode, the pump and the LSB waves can propagate to a distant location from where PDI occurred, and the beat modulation by these two waves may excite a third low-frequency oscillation (LFO). This is a channel of energy transfer among waves and between waves and particles in spectral space and in real space, such as in nonlinear or nonlocal momentum transfer via the parametric-modulational instability [1,3]. Such transfer may contribute to spectral complexity and particle heating when the LFO is a quasimode. However, the energy transfer channel via PDI has not been investigated directly.

In this Letter, we present an investigation of PDI components (pump, LSB, LFO) during radio frequency (rf) wave heating experiments on Tokyo Spherical Tokamak-2 (TST-2) [10,11]. The rf pump wave ($f_{\mathrm{pump}} = 21$ MHz) is the high-harmonic fast wave, the LSB ($f_{\mathrm{LSB}} \sim 19.25$ MHz) is either the high-harmonic fast wave or the ion Bernstein wave, and the LFO ($f_{\mathrm{LFO}} \sim 1.75$ MHz) is the ion-cyclotron quasimode (resonance with the cyclotron motion of ions) or simply forced oscillation at the beat frequency between the pump and LSB waves. Spectra of the PDI components were observed at various locations in the edge plasma, and we experimentally elucidate the nature of these PDI components. First, we describe experimental conditions and analysis procedures. Next, we show the basic properties of the PDI components. Third, we make a working assumption to discriminate resonant mode components (RMCs) from nonlinearly driven components (NDCs) at the same frequency using the bispectral analysis. Finally, we show the origin of the nearly identical spectra and discuss nonlocal transport via PDI.

TST-2 is a small spherical tokamak device with major radius $R_0 = 0.38$ m, minor radius $a \leq 0.25$ m (aspect ratio $A \geq 1.5$), and toroidal magnetic field $B_t \leq 0.3$ T. Parameters for the present experiment were $I_p < 60$ kA, $B_t \sim 0.18$ T at R_0, line averaged electron density $\bar{n}_e \sim 2$–3×10^{18} m^{-3}, and net rf input power $P_{\mathrm{net}} \leq 220$ kW

for 1 ms duration. The outboard plasma boundary is determined by the limiter ($R = 0.63$ m $\equiv R_{\rm lim}$) attached to the rf antenna. In the TST-2 rf high-harmonic fast wave experiment, PDI is frequently observed [12,13], and PDI frequency spectra were investigated by microwave reflectometry, magnetic probes (MPs), and Langmuir probes (LPs) [9]. The $f_{\rm LSB}$ decreases with B_t while keeping the relationship $f_{\rm pump} = f_{\rm LSB} + f_{\rm LFO}$, suggesting that the LFO corresponds to the ion-cyclotron quasimode (resonance with the cyclotron motion of ions) [9]. However, nearly identical spectral peaks were observed at different locations, in the scrape-off layer (SOL) plasma on the outboard side and the inboard side (where the local ion-cyclotron frequency $f_{\rm l,ci}$ is higher by a factor of 5 compared to the outboard side) measured by MPs, and in the plasma core measured by microwave reflectometry [12].

Oscillations in the toroidal magnetic field $\tilde{B}_\phi$ were measured by MPs, and oscillations in the floating potential $\tilde{\Phi}$ were measured by LPs. The MP used for reference is fixed at a major radius of $R = 0.635$ m (just outside the limiter radius) at a toroidal angle of $\phi \sim -150°$. The LP is located at $\phi = -165°$, and measurements were made at major radii $R = 0.6225$, 0.6275, 0.6325, 0.6375, and 0.6475 m. Spectral analyses based on Fourier transform were performed to investigate the properties of PDI components. We represent Fourier components with frequency f_n and wave vector $\mathbf{k}_n$ for different measurements by X_n, Y_n, and Z_n. The intensity of each component is represented by the autopower spectrum $\langle |X_n|^2 \rangle$ where $\langle\rangle$ indicates the ensemble average. The squared cross coherence $|\langle X_n Y_n^* \rangle|^2/(\langle |X_n|^2 \rangle \langle |Y_n|^2 \rangle)$ represents the correlation or phase conservation between two different measurements X_n and Y_n, and takes the value of unity when the correlation is perfect. Bispectral analysis is used to investigate the three-wave nonlinear coupling. The bispectral power $B_{1,2} \equiv \langle X_3^* Y_1 Z_2 \rangle$ takes a finite value when the three components 1, 2, and 3 are not independent, i.e., when the three-wave matching conditions $f_1 + f_2 = f_3$ and $\mathbf{k}_1 + \mathbf{k}_2 = \mathbf{k}_3$ are satisfied. If one of the three quantities X_3, Y_1, or Z_2 is independent of the other two and the matching conditions are not satisfied, the triple product oscillates in time and $B_{1,2}$ vanishes upon time averaging. The argument of complex quantity $B_{1,2}$, $\Theta_{1,2} \equiv \tan^{-1}(\Im B_{1,2}/\Re B_{1,2})$, is called the biphase. The squared bicoherence $b_{1,2}^2 \equiv |B_{1,2}|^2/(\langle |X_3|^2 \rangle \langle |Y_1 Z_2|^2 \rangle)$ is the normalized squared bispectral power, and takes the value of unity when $X_3 \propto Y_1 Z_2$. Finite $B_{1,2}$, finite $b_{1,2}$, or stable $\Theta_{1,2}$ implies the existence of a certain nonlinear relationship, such as $X_3 \propto Y_1 Z_2$. The $\Theta_{1,2}$ represents the complex phase angle of the nonlinear coupling coefficient in the coupled wave equations [i.e., $\mathcal{N}_{1,2}$ in Eq. (2)]. The typical frequency resolution of our Fourier analyses is 0.25 MHz. Distortions of analog $\tilde{\Phi}$ signals (amplitude attenuation and phase delay) by cable capacitance may occur, but the reasoning of physics in this Letter is independent of such distortions.

The autopower spectra of $\tilde{\Phi}$ at different radial locations in the vicinity of the $R_{\rm lim}$ are shown in Fig. 1(a). Considering that $T_e \sim 25 \pm 3$ eV in this region (measured by the LP), the autopower reflects the electrostatic potential energy. Four spectral peaks, corresponding to the pump, LSB, LFO, and upper sideband (USB) are clearly observed. However, the nature and origin of LSB and LFO have not been clarified experimentally. The similarity of the spectra measured at different locations indicates the existence of a radial link among respective PDI components. The autopowers in the core plasma are larger than those outside the $R_{\rm lim}$, indicating that PDI occurs inside the confined plasma boundary [12]. As shown in Fig. 1(b), the PDI components (pump, LSB, LFO) exhibit significant nonlinear coupling among each other. Three processes are considered as possible mechanisms for generating the LFO. The first possibility is local PDI, in which the LFO is generated where it is measured. In this case the $f_{\rm LFO}$ should coincide with the $f_{\rm l,ci}$. The second possibility is beat oscillation generation by the two resonant propagating modes, the pump wave and the LSB wave. The third possibility is that PDI occurs elsewhere, and the LFO propagates to the LP location with a constant phase relationship to the other PDI components. The first possibility is excluded by the fact that the frequency difference between the pump wave and the LSB wave ($\Delta f = f_{\rm pump} - f_{\rm LSB}$) does not track the $f_{\rm l,ci}$, as shown in Fig. 1(c). Propagation of the PDI components with a constant phase

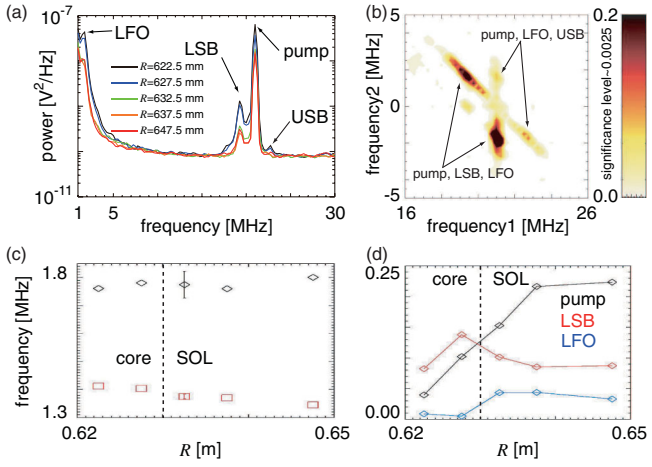

FIG. 1 (color). (a) Autopower spectra of $\tilde{\Phi}$ measured at different radial locations by LPs. Four distinctive spectral peaks of the PDI components are observed. The autopowers in the core plasma are larger than those in the SOL. (b) Contour plot of bicoherence on the f_1-f_2 plane at $R = 0.6325$ m. Significant nonlinear couplings among the PDI components are observed. (c) $f_{\rm l,ci}$ (red squares), and $\Delta f(R) = f_{\rm pump} - f_{\rm LSB}$ (black diamonds) measured with 40 kHz frequency resolution. The vertical dashed line indicates the $R_{\rm lim}$. Error bars represent data scatter. The $f_{\rm LFO}$ is different from the $f_{\rm l,ci}$. (d) Radial profiles of squared coherences (for pump and LSB) and bicoherence (for LFO). Radial coherence profiles are different among the PDI components.

relationship can be tested by coherence analysis. Figure 1(d) shows the computed $|\langle\tilde{\Phi}\tilde{B}_\phi^*\rangle|^2/(\langle|\tilde{\Phi}|^2\rangle\langle|\tilde{B}_\phi|^2\rangle)$ for the pump and LSB waves. Since LFO has few magnetic field components, and the linear coherence $\langle\tilde{\Phi}\tilde{B}_\phi^*\rangle$ is quite noisy, we use the bicoherence $|\langle\tilde{\Phi}_3^*\tilde{B}_{\phi,1}\tilde{B}_{\phi,2}\rangle|^2/(\langle|\tilde{\Phi}_3|^2\rangle\times\langle|\tilde{B}_{\phi,1}\tilde{B}_{\phi,2}|^2\rangle)$ for the LFO. The pump wave and the LFO lose coherence inside the last closed flux surface, while the phase relationship is conserved for the LSB wave. The difference in coherence profiles indicates a difference in phase conservation during wave propagation, and constant phase relationships among the PDI components are not maintained. Therefore, the third possibility is rejected.

In order to test the second possibility, we consider the nonlinear equations for the PDI components. When the nonlinear three-wave coupling condition is satisfied, the longitudinal wave is expressed as [14]

$$\tilde{\Phi}_3 = \tilde{\Phi}_{3,\mathrm{mode}} + \mathcal{N}_{1,2}\tilde{\Phi}_1\tilde{\Phi}_2 + \text{higher order terms.} \quad (1)$$

The $\tilde{\Phi}_{3,\mathrm{mode}}$ term represents the propagating RMCs, and $\mathcal{N}_{1,2}\tilde{\Phi}_1\tilde{\Phi}_2$ is the NDC where $\mathcal{N}_{1,2}$ is a complex nonlinear coupling coefficient. Longitudinal waves can couple to electromagnetic waves via the Lorentz force. Therefore, the nonlinear term $\mathcal{N}_{1,2}\tilde{\Phi}_1\tilde{\Phi}_2$ may be expressed precisely as $\sum_{k_3=k_1+k_2}(\Lambda_L\mathbf{j}_1\times\mathbf{B}_2+\Lambda_P\tilde{\Phi}_1\tilde{\Phi}_2)$ where $\Lambda_L\mathbf{j}_1\times\mathbf{B}_2$ is the Lorentz force and $\Lambda_P\tilde{\Phi}_1\tilde{\Phi}_2$ is the electrostatic ponderomotive force. When a linear relationship between $\tilde{B}_\phi$ and $\tilde{\Phi}$ can be assumed for PDI components, the Lorentz force is also proportional to $\tilde{\Phi}_1\tilde{\Phi}_2$, and the nonlinear term can be written only in terms of $\tilde{\Phi}_1\tilde{\Phi}_2$. In the weak coupling limit, a proportional relationship holds via the wave equation, Poisson equation, and charge continuity equation. This assumption is supported experimentally. Figure 2 shows the dependence of $|\tilde{\Phi}_n|^2$ on $|\tilde{B}_{\phi,n}|^2$ obtained in an rf power scan experiment, where n stands for the pump wave or the LSB wave. Clear relationships of $|\tilde{B}_{\phi,n}|^2\propto|\tilde{\Phi}_n|^2$ for both waves can be seen. Thus, the assumption $|\tilde{\mathbf{B}}_n|\propto|\tilde{\Phi}_n|$ is valid for the pump and LSB waves. In contrast, LFO has little correlation with $\tilde{B}_n$, indicating that LFO is an electrostatic oscillation. We use the nonlinear term $\mathcal{N}_{1,2}\tilde{\Phi}_1\tilde{\Phi}_2$ including the Lorentz force. It should be noted that the coupling coefficient method discussed in Ref. [15] was used successfully in deriving the nonlinear functions of potential and charge density, leading to parametric dispersion relations. Combining the linear wave equations and the charge continuity equation with the potential and the charge density, the nonlinear coefficient $\mathcal{N}_{1,2}$ including the Lorentz force can be derived.

Based on Eq. (1) we compare bispectral powers and autopowers to discriminate between RMCs and NDCs. The relationship between the bispectral and autopowers can be expressed as

$$|\tilde{\Phi}_3|^2 = \tilde{\Phi}_{3,\mathrm{mode}}\tilde{\Phi}_3^* + \mathcal{N}_{1,2}\tilde{\Phi}_1\tilde{\Phi}_2\tilde{\Phi}_3^*. \quad (2)$$

In the limit of $\tilde{\Phi}_{3,\mathrm{mode}}\to 0$ (i.e., no RMCs), the plot of $|\tilde{\Phi}_3|^2$ vs $|\tilde{\Phi}_1\tilde{\Phi}_2\tilde{\Phi}_3^*|$ should follow a straight line through the origin. This means $\tilde{\Phi}_3$ is driven entirely by the coupling of $\tilde{\Phi}_1$ and $\tilde{\Phi}_2$ (i.e., $\tilde{\Phi}_3\propto\tilde{\Phi}_1\tilde{\Phi}_2$). Without a nonlinear interaction, the biphase of $\tilde{\Phi}_1\tilde{\Phi}_2\tilde{\Phi}_3^*$ becomes random, and the comparison makes no sense. Therefore, the stability of biphase is checked and similar biphase conditions are selected. Plots of the biphase Θ of $\tilde{\Phi}_{\mathrm{pump}}\tilde{\Phi}_{\mathrm{LSB}}\tilde{\Phi}_{\mathrm{LFO}}^*$ against the bispectral powers $|\tilde{\Phi}_{\mathrm{pump}}\tilde{\Phi}_{\mathrm{LSB}}\tilde{\Phi}_{\mathrm{LFO}}^*|$ obtained in the SOL plasma are shown in Figs. 3(a) and 3(b). The wide bispectral power range originates from the temporal variation during the entire period of rf injection. No ensemble averaging was performed to obtain Fig. 3. In the high bispectral power region, the biphase is stable around $-\pi/2$. In a monochromatic wave system, the constant biphase indicates that the nonlinear relationship among the PDI components is constant regardless of temporal variation of the bispectral power. Thus, we focus on the data under stable biphase condition. Dependences of the three autopowers $|\tilde{\Phi}_{\mathrm{pump}}|^2$, $|\tilde{\Phi}_{\mathrm{LSB}}|^2$, and $|\tilde{\Phi}_{\mathrm{LFO}}|^2$ on the bispectral power, obtained at $R=0.6475$ m and $R=0.6325$ m, are shown in Figs. 3(c)–3(h), respectively. The scatter in these plots implies that the autopowers of the pump and LSB waves are sufficiently independent of the bispectral power, and the pump and LSB waves are dominated by the RMCs. The scatter could originate from temporal variations of the RMCs of the pump and LSB waves. In contrast, Figs. 3(e) and 3(h) show a proportional relationship $|\tilde{\Phi}_{\mathrm{LFO}}|^2\propto|\tilde{\Phi}_{\mathrm{pump}}\tilde{\Phi}_{\mathrm{LSB}}\tilde{\Phi}_{\mathrm{LFO}}^*|$. The scatter in Fig. 3(e) is much smaller than those in Figs. 3(c) and 3(d). If the NDC is dominant in the autopower, the proportional relationship holds regardless of the variation in the bispectral power. Therefore, the NDC is dominant in the $|\tilde{\Phi}_{\mathrm{LFO}}|^2$. The same conclusion can be drawn from Fig. 3(h). These observations confirm the picture that the LFO in the SOL is driven mainly by the nonlinear coupling of the pump and LSB waves, while the pump and LSB contain the RMCs.

We can obtain the steady state RMCs by performing ensemble averaging of plots such as those shown in Fig. 3. After ensemble averaging, the first term on the right-hand

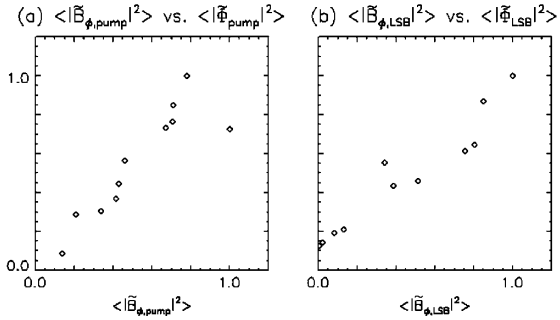

FIG. 2. Dependences of the oscillating potential power $\langle|\tilde{\Phi}|^2\rangle$ on the toroidal magnetic field power $\langle|\tilde{B}_\phi|^2\rangle$ for (a) the pump wave, and (b) the LSB wave. Powers are normalized by their maximum values. It can be seen that $\langle|\tilde{B}_\phi|^2\rangle$ is approximately proportional to $\langle|\tilde{\Phi}|^2\rangle$ for both pump and LSB waves.

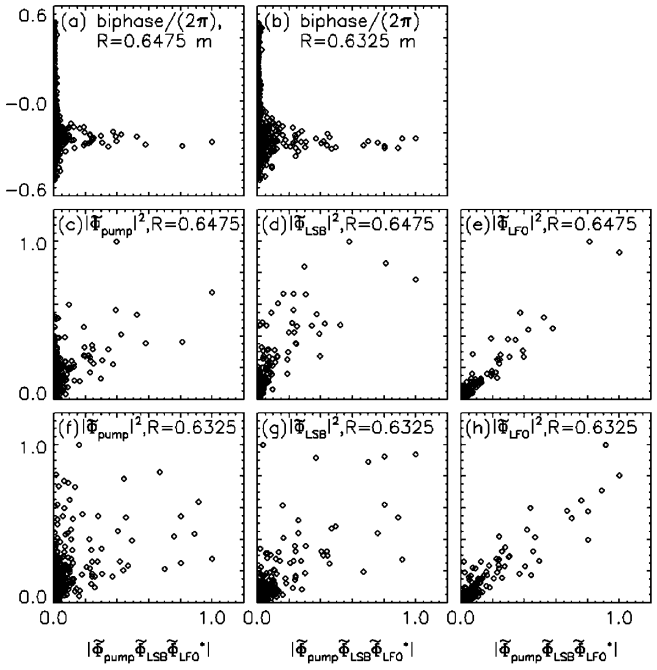

FIG. 3. Dependences of spectral functions on bispectral powers measured in the SOL plasma. (a), (b) The Θ [rad/2π]; (c), (f) $|\tilde{\Phi}_{\mathrm{pump}}|^2$; (d), (g) $|\tilde{\Phi}_{\mathrm{LSB}}|^2$; and (e), (h) $|\tilde{\Phi}_{\mathrm{LFO}}|^2$. (a), (c)–(e) and (b), (f)–(h) were measured at $R = 0.6475$ and 0.6325 m, respectively. Powers are normalized by their maximum values. Each figure is obtained from a single discharge. Dependences of the $|\tilde{\Phi}_{\mathrm{pump}}|^2$ and $|\tilde{\Phi}_{\mathrm{LSB}}|^2$ on the bispectral power are scattered [(c), (d), (f), and (g)], indicating that the pump and LSB have a significant fraction of RMCs. In contrast, the LFO power exhibits a clear linear dependence [(e) and (h)], demonstrating that the LFO is dominantly driven by the NDCs.

side of Eq. (2) should appear as an offset (averaged RMCs) on the plot. Therefore, we can conclude that no RMC exists if there is no offset. Figure 4 shows the averaged dependences of various spectral functions on the bispectral power. We selected bispectral data which are larger than 1% of the maximum value to remove the unstable biphase region. After this selection, we compare the asymptotic behaviors of $\langle|\tilde{\Phi}_3|^2\rangle$ in the limit of $\langle\tilde{\Phi}_1\tilde{\Phi}_2\tilde{\Phi}_3^*\rangle \to 0$ for the pump wave, LSB wave, and LFO in Fig. 4. Approximately linear dependences of all the autopowers on the bispectral power are seen for all cases, indicating that the PDI components have finite NDCs. However, the asymptotic values for $\langle\tilde{\Phi}_1\tilde{\Phi}_2\tilde{\Phi}_3^*\rangle \to 0$ are the highest for the pump wave, intermediate for the LSB wave, and the lowest (nearly zero) for the LFO, indicating that the fractions of the RMCs are larger for the pump wave and the LSB wave, while the NDC is dominant for the LFO. These observations are consistent with the following picture. The rf pump wave excited by the antenna produces the resonant LSB wave (and nonresonant ion-cyclotron quasimode) by PDI. The pump and LSB waves propagate from the core plasma into the SOL, and generate a beat oscillation at the f_{LFO}. This explains why nearly identical spectra are observed at various locations, including the core plasma and both inboard and outboard SOL plasmas. The beat oscillation (LFO) is a new "participant" in the spectrum, and this new driving term could be a seed to change the fluctuation structure. This provides a new nonlocal energy transfer channel for fluctuations in frequency space and in real space. This observation makes a significant contribution to the understanding of energy transfer and structural formation in nonlinear, nonequilibrium systems in nature and the laboratory.

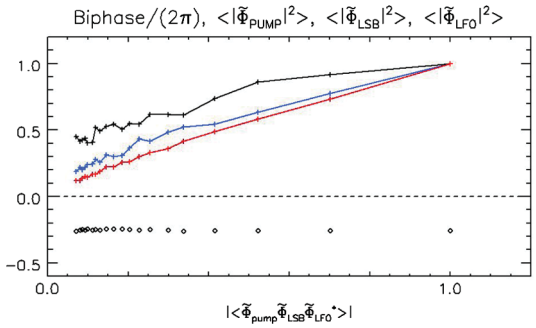

FIG. 4 (color). Dependences of spectral functions on the bispectral power in the SOL ($R = 0.6325$ m). Original data contain about 10 000 data points, and are averaged over contiguous 100 data points. Biphase [rad/(2π)] (black diamonds), $\tilde{\Phi}$ powers of the pump (black line), LSB (blue line), and LFO (red line). Powers are normalized by their maximum values. Data from 22 discharges (more than 400 spectra per discharge) under the same discharge condition are used. Linear dependences indicate that the PDI components have the NDCs. Asymptotic behaviors of $\langle|\tilde{\Phi}_3|^2\rangle$ in the limit $\langle\tilde{\Phi}_1\tilde{\Phi}_2\tilde{\Phi}_3^*\rangle \to 0$ show fractions in the RMCs. The pump and LSB contain finite RMCs, while the LFO is driven mostly by the NDCs.

This work was supported by Grants-in-Aid for Scientific Research (21226021, 21246137) of JSPS, Japan.

*nagashima@k.u-tokyo.ac.jp

[1] P. Diamond, S.-I. Itoh, K. Itoh, and T. Hahm, Plasma Phys. Controlled Fusion **47**, R35 (2005).
[2] A. Fujisawa, Nucl. Fusion **49**, 013 001 (2009).
[3] Y. Nagashima *et al.*, Phys. Plasmas **16**, 020 706 (2009).
[4] K. Kuroda, *Nonlinear Optics (in Japanese)* (Corona Publishing, Bunkyo, Tokyo, 2008).
[5] T. Suzuki and S. Inutsuka, J. Geophys. Res. **111**, A06101 (2006).
[6] M. Porkolab and R. Chang, Rev. Mod. Phys. **50**, 745 (1978).
[7] F. Chen, *Introduction to Plasma Physics and Controlled Fusion* (Plenum Press, New York and London, 1984).
[8] J. Wilgen *et al.*, Rev. Sci. Instrum. **77**, 10E933 (2006).
[9] T. Oosako *et al.*, Nucl. Fusion **49**, 065 020 (2009).
[10] Y. Takase *et al.*, Nucl. Fusion **41**, 1435 (2001).
[11] A. Ejiri *et al.*, Nucl. Fusion **49**, 065 010 (2009).
[12] T. Yamada *et al.*, Rev. Sci. Instrum. **78**, 083 502 (2007).
[13] Y. Adachi *et al.*, Rev. Sci. Instrum. **79**, 10F507 (2008).
[14] R. Aamodt, Phys. Rev. **138**, A45 (1965).
[15] P. Aliev, V. Silin, and C. Watson, Sov. Phys. JETP **23**, 626 (1966).